Catalysis Today xxx (2015) xxx–xxx

Contents lists available at ScienceDirect

Catalysis Today

journal homepage: www.elsevier.com/locate/cattod

Superior nanoporous graphitic carbon nitride photocatalyst coupled with CdS quantum dots for photodegradation of RhB

Qianjing Fan [a], Yanni Huang [a], Chi Zhang [a,b], Jianjun Liu [a,*], Lingyu Piao [b], Yingchun Yu [a], Shengli Zuo [a], Baoshan Li [a]

[a] State Key Laboratory of Chemical Resource Engineering, Beijing University of Chemical Technology, Beijing 100029, PR China
[b] National Center for Nanoscience and Technology, Beijing 100190, PR China

ARTICLE INFO

Article history:
Received 4 May 2015
Received in revised form 21 July 2015
Accepted 6 August 2015
Available online xxx

Keywords:
Nanoporous carbon nitride
CdS quantum dots
Photodegradation
Visible light

ABSTRACT

Nanoporous graphitic carbon nitride (npg-C_3N_4) shows much higher photocatalytic activities than bulk g-C_3N_4. Npg-C_3N_4 was used to couple with CdS quantum dots (QDs) by a simple deposition method to further increase the photocatalytic activities of the photocatalyst. The obtained photocatalyst was characterized by XRD, FT-IR, and XPS techniques; nitrogen adsorption isotherms, SEM and TEM images; and UV–vis DRS and Photoluminescence spectra. Results showed that the CdS QDs had been successfully deposited onto the surface of npg-C_3N_4 with a good dispersion, and the two components formed stable composites because the CdS QDs can be anchored by the rolled and curled edges of npg-C_3N_4. The as-prepared CdS QDs/npg-C_3N_4 composites not only exhibited extended optical absorptions of visible light (up to 600 nm) and enhanced photocatalytic activity for the photodegradation of Rhodamine B than each of the components, but also showed good catalytic stability.

1. Introduction

The extensive use in many fields and unintended release into the environment of synthetic dyes cause considerable environmental pollution and serious health-risk to human. As the pollutants of synthetic dyes in wastewater are chemical stable, a wide range of methods has been developed for the removal of these pollutants [1]. Photocatalysis using semiconductors, as one of the most effective methods, has received considerable attention during the past decades [2–4]. TiO_2 is the most widely studied photocatalyst due to its non-toxicity, good stability and excellent photocatalytic activity. But TiO_2 is not a visible light active photocatalyst because of its wide band gap (3.2 eV) [5]. Exploring new photocatalytic materials with photocatalytic activity under visible light is of great interest. Recently, a polymeric graphitic carbon nitride (g-C_3N_4) composed of carbon, nitrogen, and some minor hydrogen content only, was introduced as a metal-free photocatalyst for solar-driven applications, such as organic pollutant degradation [6], water splitting [7–9], and CO_2 reduction [10–12] in the visible light region. This organic semiconductor offers new opportunities for photocatalysis due to its cheap availability, high stability, and visible light response. However, the photocatalytic activities of pristine g-C_3N_4 are seriously limited by its intrinsic drawbacks, including relatively low surface area, fast charge recombination, and poor mass diffusion/transfer [13,14]. Many methods have been developed to enhance its photocatalytic performance, including texture modification [15–19], element doping [20–22] and noble metal deposition [23], and constructing heterojunctions with other materials [24–27]. Among these methods, introducing nanoporous [28–31] in g-C_3N_4 has been demonstrated a facile and efficient pathway to promote charge migration and separation, as well as the mass diffusion/transfer during photoredox reactions, greatly enhancing the photocatalytic performance. Our recent study [32] also revealed that nanoporous g-C_3N_4 (npg-C_3N_4) with large surface area exhibits much higher photocatalytic activity than pristine g-C_3N_4. Considering combining with other semiconductors has been demonstrated an effective way to inhibit the recombination of photogenerated electron–hole pairs, it was supposed that introducing another visible light response semiconductor to the texture modified npg-C_3N_4 can further improve the photocatalytic activity of the catalyst.

CdS, as a well-known II–IV semiconductor, has been attracting increasing attention as a visible-light catalyst due to its narrow band gap of 2.4 eV [33]. However, several drawbacks still limit the photocatalytic efficiency on pure CdS nanoparticles. For example, small CdS particles can easily aggregate into large particles,

* Corresponding author. Tel.: +86 10 64431056; fax: +86 10 64434898.
E-mail address: jjliu717@aliyun.com (J. Liu).

http://dx.doi.org/10.1016/j.cattod.2015.08.006
0920-5861/

resulting in smaller surface area and higher recombination rate of photogenerated electrons and holes. Additionally, CdS seriously suffers from photocorrosion as S^{2-} in CdS tends to be self-oxidized by photogenerated holes during the photocatalytic reaction [34]. Several approaches have been developed to solve these problems. For instance, CdS was coupled with various semiconductors (TiO_2 [35], ZnO [36], MoS_2 [37], etc.) or noble metals [38,39] to promote the separation of photogenerated charge carriers. By coating with polymeric materials (such as polyaniline [40] and resin [41]) or carbon films [42] to form core/shell nanostructure, the problem of CdS photocorrosion can be mostly inhibited. Recently, several works have reported that the photocatalyst coupled by CdS and g-C_3N_4 shows better photocatalytic performance than the pure g-C_3N_4 and CdS for H_2 generation because of the high efficiency of the separation of photogenerated charge carriers [43–47]. Therefore, the combination of g-C_3N_4 and CdS can deal with the drawbacks of each other simultaneously [48]. But the reported CdS/g-C_3N_4 composites synthesized by using the pristine g-C_3N_4 with low surface area to couple with CdS exhibited relatively low photocatalytic activity. Very recently, Zheng et al. [49] used hollow carbon nitride spheres (HCNS) to synthesize CdS/g-C_3N_4 composites, which showed excellent photocatalytic activity and stability. But the use of g-C_3N_4 with nanostructures to construct CdS/g-C_3N_4 composites is still limited.

Herein, the npg-C_3N_4 with rolled layer edges and excellent photocatalytic activity [32] was used to couple with CdS quantum dots for further improving the photocatalytic activity. The unique structure of npg-C_3N_4 not only can provide more catalytic active sites, but also can direct a good dispersion of the CdS QDs and inhibit the aggregation of CdS QDs. The CdS QDs/npg-C_3N_4 composites were characterized in terms of chemical structure, morphology, optical and electronic properties. The photocatalytic activity of the obtained samples was tested by evaluating the degradation of Rhodamine B (RhB) dye under visible light illumination, and the CdS QDs optimum content was investigated.

2. Experimental

2.1. Synthesis of npg-C_3N_4

All chemicals were of analytical grade without further treatment. Npg-C_3N_4 was synthesized by a template-induced method as we have reported before [32]. In a typical synthetic procedure, 5.0 g melamine and 2.5 g Triton X-100 were added into 100 mL distilled water, and then the mixture was heated in an oil bath at 100 °C with stirring for 1 h under refluxing. Then 2 mL concentrated sulfuric acid (98 wt%) was added to the solution dropwise while the white precipitate gradually formed, and the mixture was stirred at 100 °C for another hour. After naturally cooling down to room temperature, the precipitate was filtrated and washed several times with distilled water to remove Triton X-100, then dried in an oven at 80 °C overnight. The obtained sample was put into an alumina crucible with a cover and then heated to 500 °C in a muffle furnace for 2 h with a heating rate of 2 °C min^{-1}, and further heat treatment was set at 580 °C for another 2 h.

2.2. Synthesis of CdS QDs

CdS QDs were prepared in the aqueous phase with TGA (thioglycollic acid) as stabilizer by adding 0.5 mL TGA to a 17.5 mmol $CdCl_2{\cdot}2.5H_2O$ (200 mL) solution with at pH 10 adjusted by the addition of 1 mol L^{-1} NaOH solution. The Na_2S solution obtained by dissolving 0.84 g $Na_2S{\cdot}9H_2O$ in 10 mL water was added to the solution, and then the mixture was stirred at 60 °C for 1 h. Subsequently, the solution was centrifuged, and the CdS QDs were extracted and rinsed with distilled water. The obtained sample was redispersed in distilled water to obtain a pure CdS QDs aqueous solution.

2.3. Synthesis of CdS QDs/npg-C_3N_4 composites

CdS QDs/npg-C_3N_4 composite photocatalysts were prepared as following: the as-prepared npg-C_3N_4 powder (0.3 g) was added to 20 mL CdS QDs solutions containing different amounts of CdS QDs and stirred for 1 h. Then 10 mL acetone was added to the solution to make CdS QDs deposit onto the surface of npg-C_3N_4. After being stirred for 24 h, the product was collected by centrifugation, followed by drying in an oven at 80 °C overnight. Finally, the samples were heated at 300 °C in a muffle furnace for 1 h. Thus, CdS QDs/npg-C_3N_4 composites with weight percentages of CdS QDs of 2.5, 5, 10, 15, and 20 wt% were prepared, denoted as CdS/CN-2.5%, 5%, 10%, 15%, and 20%, respectively. For comparison, the pure CdS QDs also treated by the same route.

2.4. Characterization

X-ray diffraction (XRD) patterns were collected in a Bruker D8FOCUS powder diffractometer with Cu Kα irradiation (λ = 0.15406 nm). X-ray photoelectron spectroscopy (XPS) data were measured by an ESCALAB-250 with monochromated Al Kα radiation. Transmission electron microscopy (TEM) and high-resolution TEM (HRTEM) images were taken with Tecnai G220 microscope and JEOL-3010 microscope, respectively. Scanning electron microscopy (SEM) images Hitachi S4700 and the elemental compositions were analyzed by the energy dispersive spectrometer (EDS) (INCA Energy, OXFORD). Nitrogen sorption measurements were accomplished with N_2 at 77 K after degassing the samples at 300 °C under vacuum for 3 h using a Quantachrome Quadrasorb SI-MP porosimeter. The specific surface area was calculated by applying the Brunauer–Emmett–Teller (BET) model to analyze the adsorption data. UV–vis absorption spectra were measured using a Shimadzu UV3600 spectrophotometer. The photoluminescence (PL) spectra were performed on a Hitachi F7000 fluorescence spectrophotometer with photomultiplier tube voltage of 400 V and scanning speed of 1200 nm min^{-1}.

2.5. Photocatalytic evaluation

The photocatalytic activity of the samples was evaluated by degradation of RhB under visible light irradiation. A 500 W Xenon lamp (Institute of Electric Light Source, Beijing) with 400 nm cut-off filter was chosen as a visible light source. The temperature of the reaction solution was kept at 20 °C by means of a cooling water sleeve surrounding the lamp. The distance between the light source and the surface of the reaction solution was 15 cm. In a typical experiment, 0.1 g photocatalyst was suspended in RhB aqueous solution (100 mL, 10 mg L^{-1}), and then stirred in the dark for 1 h to reach the adsorption–desorption equilibrium. During the visible light irradiation, an aliquot of 5 mL containing the sample was taken from the reaction suspensions at given time intervals, and then centrifuged to remove the photocatalyst particles. Subsequently, the solutions were measured with the UV–vis spectrophotometer at wavelength of 554 nm. The concentration changes were described by C/C_0, where C_0 is the initial concentration of RhB (after subtraction of the concentration of RhB which was adsorbed to the catalysts) and C is the remained concentration of RhB. The RhB degradation percent (Dp) was determined by $Dp = [1 - (C/C_0)] \times 100\%$.

Please cite this article in press as: Q. Fan, et al., Superior nanoporous graphitic carbon nitride photocatalyst coupled with CdS quantum dots for photodegradation of RhB, Catal. Today (2015), http://dx.doi.org/10.1016/j.cattod.2015.08.006

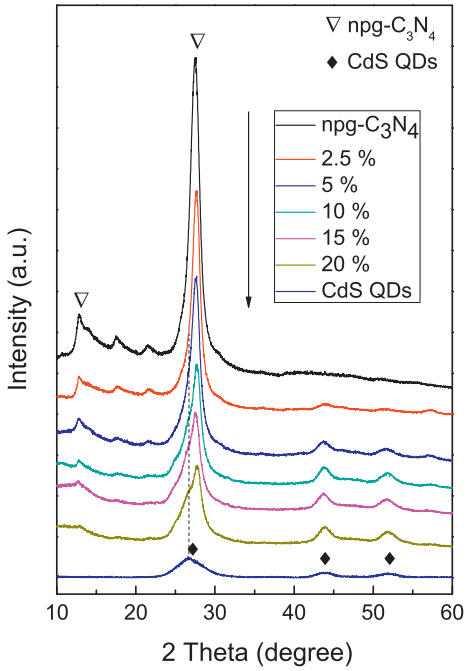

Fig. 1. XRD patterns of npg-C_3N_4, pure CdS QDs and CdS QDs/npg-C_3N_4 composites.

3. Results and discussion

3.1. Characterization of CdS QDs/npg-C_3N_4 composites

The XRD patterns of the as prepared npg-C_3N_4, pure CdS QDs and CdS QDs/npg-C_3N_4 composites are shown in Fig. 1. For pure npg-C_3N_4, the two pronounced diffraction peaks at 27.4° and 13.1° are considered to the typical graphitic interlayer (0 0 2) peak with d = 0.326 nm and the in-plane structural packing motif (1 0 0) with d = 0.672 nm, respectively [50]. The pure CdS QDs exhibits three peaks at 26.7°, 43.9°, and 51.2°, which correspond to the face-centered cubic crystalline structure CdS (JCPDS No. 89-0440) [43]. The crystalline size of CdS QDs was calculated as 8.1 nm by Debye–Scherrer equation. The typical graphitic interlayer (0 0 2) peak at 27.4° of g-C_3N_4 can be easily found in all the CdS QDs/npg-C_3N_4 composites. Although the peaks of CdS QDs are not very obvious in the CdS QDs/npg-C_3N_4 composites with low CdS QDs doping amount (2.5 wt%), the existence of CdS QDs phase in the composites can be demonstrated by the phenomenon that the intensity of CdS QDs peaks increase with the increase of CdS QDs doping amount.

The chemical composition of the CdS QDs/npg-C_3N_4 composites was determined by energy dispersive spectroscopy (EDS) techniques. The typical EDS pattern of CdS/CN-10% was shown in Fig. A.1, and the element contents of all the samples were listed in Table A.1. As a result, the main elements of the CdS QDs/npg-C_3N_4 composites are C, N, S, and Cd, and the actual CdS QDs doping amounts in the composites are mostly in consistent with the theoretical doping amounts. This result demonstrates that CdS QDs have been deposited onto the surface of npg-C_3N_4. The chemical states of C, N, Cd and S in the CdS/CN-10% were further characterized by XPS (Fig. 2). The C 1s peak (Fig. 2a) can be fitted into two peaks. The peak at 284.8 eV is typically ascribed to sp^2 C–C bonds of pure carbon such as graphite or amorphous carbon, and the peak at 288.2 eV is identified as sp^2-bonded carbon in N-containing aromatic rings (N–C=N) [9]. In Fig. 2b, three peaks are deconvoluted for N 1s spectra. The peak centering at 398.4 eV and 399.1 eV are attributed to the sp^2-hybridized nitrogen involved in triazine rings (C–N=C) and the tertiary nitrogen N–$(C)_3$ groups, respectively. The weak peak at 401 eV indicates the presence of amino functions (C–N–H), originating from the incomplete condensation of poly(tri-s-triazine)

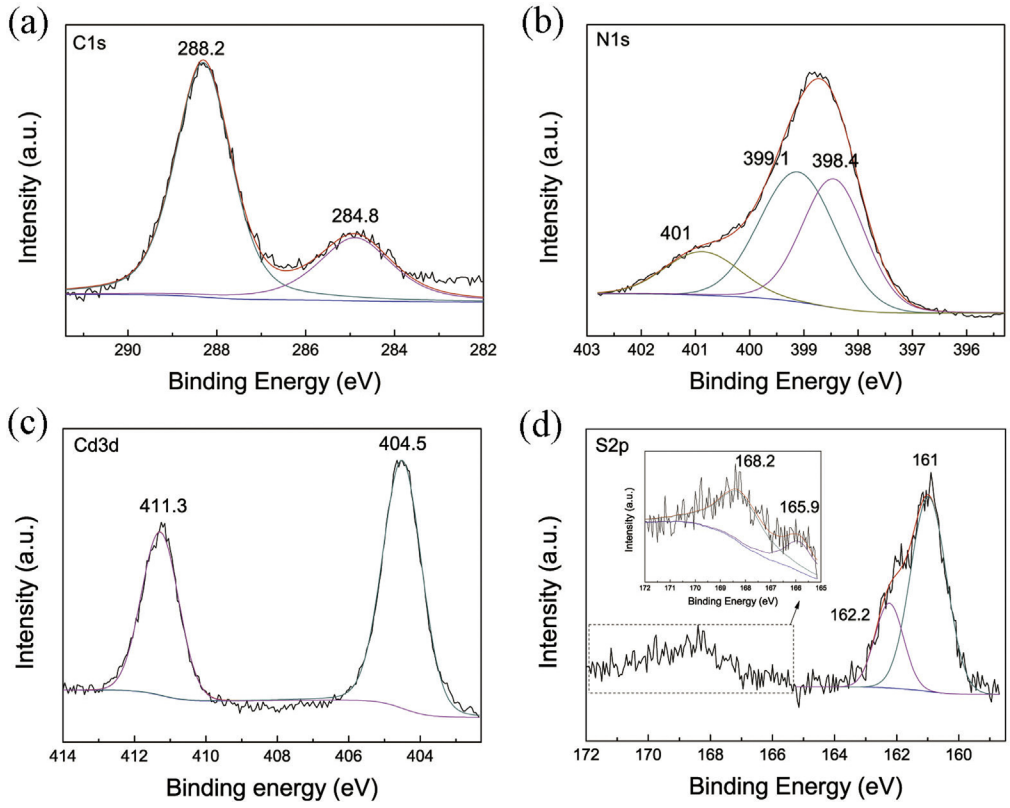

Fig. 2. High-resolution XPS spectra of (a) C1s, (b) N1s, (c) Cd3d and (d) S2p of CdS/CN-10%.

Please cite this article in press as: Q. Fan, et al., Superior nanoporous graphitic carbon nitride photocatalyst coupled with CdS quantum dots for photodegradation of RhB, Catal. Today (2015), http://dx.doi.org/10.1016/j.cattod.2015.08.006

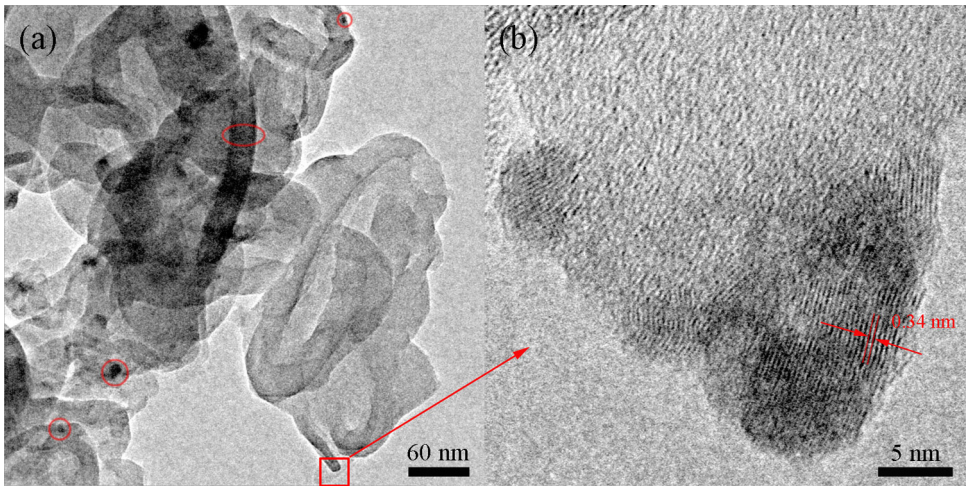

Fig. 3. HRTEM images of the sample of CdS/CN-10% with different magnifications.

structures [51]. The peaks for Cd 3d were observed at 404.5 eV and 411.3 eV (Fig. 2c) can be assigned to the Cd^{2+} ions of the CdS QDs. Fig. 2d shows the peak for S 2p is deconvolved into four peaks at 161 eV, 162.2 eV, 165.9 eV and 168.2 eV. The peaks at 161 eV and 162.2 eV are identified as the sulfide in CdS QDs [43,44]. The weak peak at 165.9 eV can be attributed to that little sulfur incorporated into the position of carbon to give rise to few S–N bonds, according the previous report [52]. The peak at 168.2 eV is regarded as some sulfate radicals generated during the process of calcination.

The morphology and microstructure of the samples were investigated by SEM and TEM. The TEM images of the npg-C_3N_4 and CdS QDs are shown in Fig. A.2. The CdS QDs show uniform grain size about 3 nm, and the npg-C_3N_4 show layered structures with rolled and buckled edges, corresponding to our previous report [32]. The TEM images of CdS QDs/npg-C_3N_4 composites are showed in Fig. A.3, from which can be found that the CdS QDs have been successfully deposited onto the surface of npg-C_3N_4 support with a good dispersion. The particle size of CdS QDs in the composites is around 10 nm, corresponding to the result of pure CdS QDs calculated from XRD patterns. This result indicates that the little increased particle size of CdS QDs can be attributed to the aggregation of the CdS QDs during the deposition by using acetone and the heating treatment [43]. More details about the combination in the composites are shown in the HRTEM images of CdS/CN-10% (Fig. 3). The typical positions of CdS QDs, marked by red circles in Fig. 3a, show that the CdS QDs can be anchored by the rolled and curled edges of npg-C_3N_4. The lattice spacing of 0.34 nm marked in Fig. 3b corresponds to the (1 1 1) lattice plane of cubic CdS crystal. These results demonstrate the CdS QDs and the npg-C_3N_4 in the composites have a stable combination. The SEM image of CdS/CN-10% (Fig. A.3a) indicates that the composites still exhibit the porous structure. Nitrogen sorption analysis was used to further evaluate the porosity of the samples (Fig. 4). The isotherms of the CdS QDs/npg-C_3N_4 composites all show similar hysteresis loops with the npg-C_3N_4 range at $p/p_0 = 0.8–1.0$, corresponding to the macroporous system, and the corresponding BJH pore size distribution curves (Fig. A.4) of CdS QDs/npg-C_3N_4 composites determined from the adsorption branch of the isotherms are still centered at around 40–60 nm, similar to that of pure npg-C_3N_4. The BET surface areas of CdS QDs/npg-C_3N_4 composites show little decrease with the increase of CdS QDs content (npg-C_3N_4, CdS/CN-2.5%, CdS/CN-5%, CdS/CN-10%, and CdS/CN-20% are 66.7, 61.9, 61.8, 52.8, and 49.3 $m^2\ g^{-1}$, respectively), indicating that introduced CdS QDs have partially blocked the nanopores in npg-C_3N_4.

The UV–vis spectra of the as prepared npg-C_3N_4, pure CdS QDs and CdS QDs/npg-C_3N_4 composites are shown in Fig. 5. The pure npg-C_3N_4 exhibits an absorption edge at 458 nm and the pure CdS QDs have an absorption edge at 535 nm, corresponding to the results reported in the literature.[43,44] For CdS QDs/npg-C_3N_4 composites, there was a red shift in the absorption edge and an enhanced absorbance in the visible light region ranging from 400 to 700 nm with the increase of the CdS QDs content, comparing with the absorbance spectrum of pure npg-C_3N_4. This result can be attributed to the enhanced separation efficiency of charge pairs

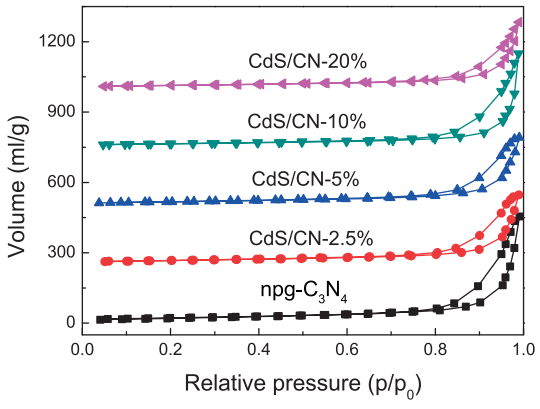

Fig. 4. N_2 adsorption/desorption isotherms of npg-C_3N_4 and CdS QDs/npg-C_3N_4 composites.

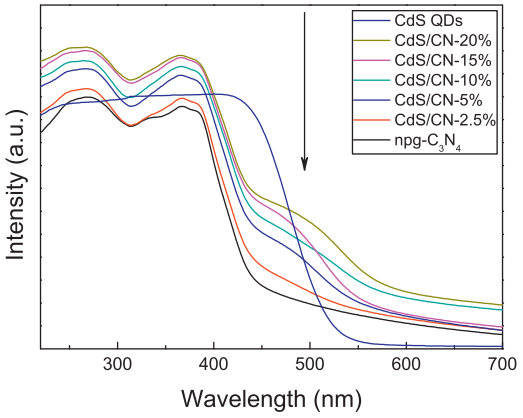

Fig. 5. UV–vis spectra of npg-C_3N_4, pure CdS QDs and CdS QDs/npg-C_3N_4 composites.

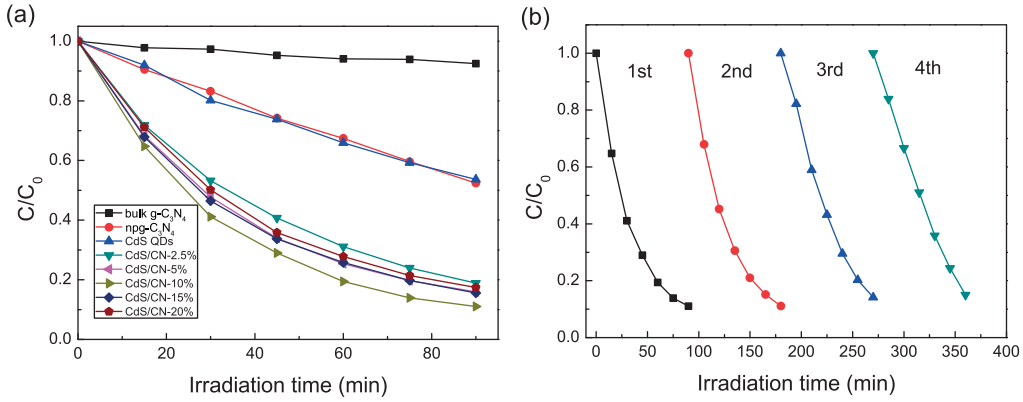

Fig. 6. (a) Photocatalytic degradation of RhB for npg-C_3N_4, pure CdS QDs and CdS QDs/npg-C_3N_4 composites and (b) cycling runs for the photocatalytic degradation of RhB in the presence of the sample of CdS/CN-10%.

induced by combination of CdS QDs and npg-C_3N_4 [53] and the decreased the band gaps of npg-C_3N_4 caused by little sulfur incorporated into the lattice of npg-C_3N_4 [20,52].

3.2. Evaluation of photocatalytic activity of CdS QDs/npg-C_3N_4 composites

The photocatalytic activities of all the samples were evaluated for Rhodamine B (RhB) photodegradation under visible light ($\lambda > 400$ nm) irradiation for 90 min. The bulk g-C_3N_4 synthesized by directly heating melamine at 550 °C for 4 h also was evaluated for comparison. From Fig. 6a, the npg-C_3N_4 show higher photodegradation efficiency than bulk g-C_3N_4 because of the large BET surface area of npg-C_3N_4. The CdS QDs/npg-C_3N_4 composites show much higher photodegradation efficiency (Dp = 71.1–88.2%) of RhB than that of pure npg-C_3N_4 (Dp = 47.6%) and CdS QDs (Dp = 46.5%). Even with only 2.5 wt% CdS QDs deposited on the npg-C_3N_4, the composite shows high photodegradation efficiency with 71.1%. This result demonstrates that the combination of CdS QDs and npg-C_3N_4 can drastically increase the photodegradation efficiency. Besides, the sample of CdS/CN-10% shows the highest photodegradation rate, which will decrease if the content of CdS QDs keep increasing. This is because the BET surface areas decreased with the increase of CdS content and CdS QDs showed partial aggregation when the CdS QDs content is over 10% (Fig. A.3). The stability of photocatalytic activity was investigated by using the sample of CdS/CN-10% as the photocatalyst example (as shown in Fig. 6b). In the cycle evaluations, the photocatalytic activity of the catalyst show little decrease after four cycle evaluations, and the XRD patterns (as shown in Fig. A.5) of the used photocatalyst after 4th cycling experiment are almost the same as that of the fresh photocatalyst. These results demonstrate the high stability of the CdS QDs/npg-C_3N_4 composite under our experiment conditions, and the photocorrosion reaction of CdS QDs [34] can be greatly inhibited by combining the CdS QDs with npg-C_3N_4.

Generally, decolorization does not mean that the dyes have been completely oxidized into harmless final products such as H_2O and CO_2. In order to determine the photodegradation of RhB is a decolorization or mineralization process, the variation of UV–vis absorption spectra of RhB degradation using CdS/CN-10% is shown in Fig. A.6. The characteristic absorption band of RhB at 554 nm decreased significantly with increasing irradiation time, accompanied by a remarkable blue-shift of the maximum absorption peak. The stepwise blue-shift of the main peak from 554 to 496 nm can be attributed to the step-by-step de-ethylation of RhB molecule, while the decrease in absorbance indicates the destruction of the conjugated structure [6]. These absorption peaks completely disappeared after illumination for 8 h, suggesting the chromophoric structure of the RhB dye can be decomposed.

3.3. Mechanism of photocatalytic activity enhancement

The photocatalytic degradation mechanism of dye pollutants by CdS QDs/npg-C_3N_4 composites was investigated by introducing 10 mM isopropyl alcohol (IPA), triethanolamine (TEOA), and p-benzoquinone (BQ), which are known as effective •OH, holes, and $•O_2^-$ scavengers for photocatalytic reaction, respectively [6,7]. As shown in Fig. 7a, the photodegradation activity was

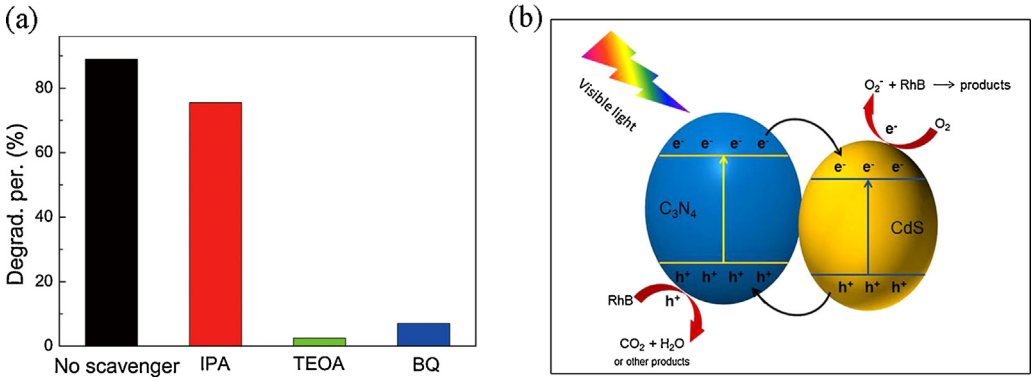

Fig. 7. (a) Effect of different scavengers on the RhB degradation in the presence of CdS/CN-10% and (b) schematic of photogenerated charge transfer in the CdS QDs/npg-C_3N_4 system under visible light.

Please cite this article in press as: Q. Fan, et al., Superior nanoporous graphitic carbon nitride photocatalyst coupled with CdS quantum dots for photodegradation of RhB, Catal. Today (2015), http://dx.doi.org/10.1016/j.cattod.2015.08.006

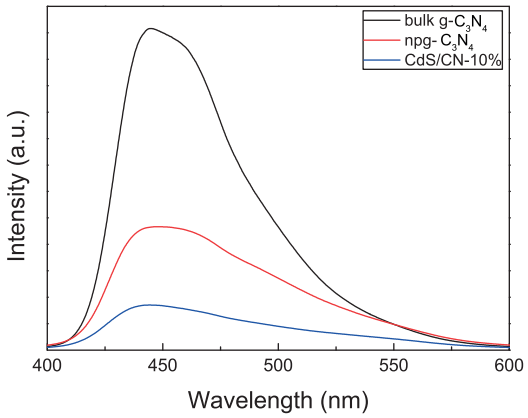

Fig. 8. PL spectra of npg-C_3N_4 and the CdS QDs/npg-C_3N_4 composites.

remarkably suppressed after adding TEOA or BQ into the reaction system, while the photodegradation activity only show little decrease after adding IPA into the reaction system. This result indicates that the holes and $^{\bullet}O_2^-$ are the main oxidative species in the photocatalytic process. Based on the result, the photogenerated charge transfer in the CdS QDs/npg-C_3N_4 composites is proposed and illustrated in Fig. 7b. It has reported that the conduction band (CB) edge potential of g-C_3N_4 is more negative than that of CdS, whereas the valence band (VB) edge potential of CdS is more positive than that of g-C_3N_4 [44,45]. Under the excitation of visible light, the photogenerated electrons can transfer from the g-C_3N_4 surfaces to CdS, and the photogenerated holes transfer from the CdS surfaces to robust g-C_3N_4. Therefore, the recombination of photogenerated charge pairs can be effectively inhibited and the charge separation efficiency can be enhanced. Especially, the rapid migration of photogenerated holes on CdS can greatly inhibited the photocorrosion of CdS due to hole oxidation. This result can be also demonstrated by the photoluminescence (PL) spectra of the samples with an excitation wavelength of 325 nm, as shown in Fig. 8. The main emission peak is centered at about 447 nm for bulk g-C_3N_4, which can be attributed to the recombination of electron–hole pairs in bulk g-C_3N_4. The fluorescence intensity of npg-C_3N_4 decreases markedly than that of bulk g-C_3N_4 because the porous structure facilitates the separation of the photogenerated electron–hole pairs. The fluorescence intensity is further decreased for the CdS QDs/npg-C_3N_4 composite, demonstrating the more efficient transfer of photogenerated electrons or holes between npg-C_3N_4 and CdS QDs.

4. Conclusions

In summary, a series of CdS quantum dot-coupled nanoporous graphitic carbon nitride photocatalysts were synthesized by a simple deposition method. The as-prepared CdS QDs/npg-C_3N_4 composites still kept large surface areas, and the CdS QDs could be anchored on the surface of npg-C_3N_4 with a good dispersion. Besides, the optical absorption edges of CdS QDs/npg-C_3N_4 composites exhibited a red shift (over 600 nm) and stronger absorption of the visible light. As a result, the combination of CdS QDs and npg-C_3N_4 realized a high efficient separation of the photogenerated charge carriers and inhibited the photocorrosion of CdS. The CdS QDs/npg-C_3N_4 composites showed enhanced photocatalytic activities for the degradation of RhB under visible light irradiation, and the optimal CdS QDs doping content was found to be 10 wt% in our system. This work may give ideas for the design and synthesis other visible light active and stable photocatalysts by taking both structural characteristics and intrinsic catalytic properties of co-catalysts into consideration.

Acknowledgement

This work was financially supported by the Natural Science Foundation of China under Grant no. 10972025.

Appendix A. Supplementary data

Supplementary data associated with this article can be found, in the online version, at http://dx.doi.org/10.1016/j.cattod.2015.08.006.

References

[1] E. Forgacs, T. Cserháti, G. Oros, Environ. Int. 30 (2004) 953.
[2] S. Chowdhury, R. Balasubramanian, Appl. Catal. B: Environ. 160–161 (2014) 307.
[3] X. Lang, X. Chen, J. Zhao, Chem. Soc. Rev. 43 (2014) 473.
[4] C.-C. Wang, J.-R. Li, X.-L. Lv, Y.-Q. Zhang, G. Guo, Energy Environ. Sci. 7 (2014) 2831.
[5] M. Pelaez, N.T. Nolan, S.C. Pillai, M.K. Seery, P. Falaras, A.G. Kontos, P.S.M. Dunlop, J.W.J. Hamilton, J.A. Byrne, K. O'Shea, M.H. Entezari, D.D. Dionysiou, Appl. Catal. B: Environ. 125 (2012) 331.
[6] Y. Cui, Z. Ding, P. Liu, M. Antonietti, X. Fu, X. Wang, Phys. Chem. Chem. Phys. 14 (2012) 1455.
[7] X. Wang, K. Maeda, A. Thomas, K. Takanabe, G. Xin, J.M. Carlsson, K. Domen, M. Antonietti, Nat. Mater. 8 (2009) 76.
[8] G. Zhang, S. Zang, X. Wang, ACS Catal. 5 (2015) 941.
[9] Z. Lin, X. Wang (Eds.), Angew. Chem. Int. 52 (2013) 1735.
[10] J. Qin, S. Wang, H. Ren, Y. Hou, X. Wang, Appl. Catal. B: Environ. 179 (2015) 1.
[11] G. Zhang, Z.-A. Lan, X. Wang, ChemCatChem 7 (2015) 1422.
[12] R. Kuriki, K. Sekizawa, O. Ishitani, K. Maeda (Eds.), Angew. Chem. Int. 54 (2015) 2406.
[13] X. Wang, S. Blechert, M. Antonietti, ACS Catal. 2 (2012) 1596.
[14] Y. Zhang, T. Mori, J. Ye, Sci. Adv. Mater. 4 (2012) 282.
[15] A. Thomas, A. Fischer, F. Goettmann, M. Antonietti, J.-O. Muller, R. Schlogl, J.M. Carlsson, J. Mater. Chem. 18 (2008) 4893.
[16] Y. Cui, Z. Ding, X. Fu, X. Wang (Eds.), Angew. Chem. Int. 51 (2012) 11814.
[17] J. Zhang, M. Zhang, L. Lin, X. Wang (Eds.), Angew. Chem. Int. 54 (2015) 6297.
[18] Y. Zheng, L. Lin, X. Ye, F. Guo, X. Wang (Eds.), Angew. Chem. Int. 53 (2014) 11926.
[19] D. Zheng, C. Huang, X. Wang, Nanoscale 7 (2015) 465.
[20] G. Liu, P. Niu, C. Sun, S.C. Smith, Z. Chen, G.Q. Lu, H.-M. Cheng, J. Am. Chem. Soc. 132 (2010) 11642.
[21] G. Zhang, C. Huang, X. Wang, Small 11 (2015) 1215.
[22] Y. Wang, H. Li, J. Yao, X. Wang, M. Antonietti, Chem. Sci. 2 (2011) 446.
[23] Y. Li, X. Xu, P. Zhang, Y. Gong, H. Li, Y. Wang, RSC Adv. 3 (2013) 10973.
[24] Y. Hou, A.B. Laursen, J. Zhang, G. Zhang, Y. Zhu, X. Wang, S. Dahl, I. Chorkendorff (Eds.), Angew. Chem. Int. 52 (2013) 3621.
[25] S. Wang, J. Lin, X. Wang, Phys. Chem. Chem. Phys. 16 (2014) 14656.
[26] K. Dai, L. Lu, C. Liang, Q. Liu, G. Zhu, Appl. Catal. B: Environ. 156–157 (2014) 331.
[27] Y. Hou, Y. Zhu, Y. Xu, X. Wang, Appl. Catal. B: Environ. 156–157 (2014) 122.
[28] Q. Gu, Y. Liao, L. Yin, J. Long, X. Wang, C. Xue, Appl. Catal. B: Environ. 165 (2015) 503.
[29] Z. Zhao, Y. Dai, J. Lin, G. Wang, Chem. Mater. 26 (2014) 3151.
[30] J. Xu, Y. Wang, Y. Zhu, Langmuir 29 (2013) 10566.
[31] M. Zhang, J. Xu, R. Zong, Y. Zhu, Appl. Catal. B: Environ. 147 (2014) 229.
[32] Q. Fan, J. Liu, Y. Yu, S. Zuo, RSC Adv. 4 (2014) 61877.
[33] J. Ran, J. Yu, M. Jaroniec, Green Chem. 13 (2011) 2708.
[34] Q. Li, B. Guo, J. Yu, J. Ran, B. Zhang, H. Yan, J.R. Gong, J. Am. Chem. Soc. 133 (2011) 10878.
[35] J. Luo, L. Ma, T. He, C.F. Ng, S. Wang, H. Sun, H.J. Fan, J. Phys. Chem. C 116 (2012) 11956.
[36] C. Eley, T. Li, F. Liao, S.M. Fairclough, J.M. Smith, G. Smith, S.C.E. Tsang (Eds.), Angew. Chem. Int. 53 (2014) 7838.
[37] J. Zhang, Z. Zhu, X. Feng, Chem. Eur. J. 20 (2014) 10632.
[38] X. Wang, C. Liow, D. Qi, B. Zhu, W.R. Leow, H. Wang, C. Xue, X. Chen, S. Li, Adv. Mater. 26 (2014) 3506.
[39] S. Han, L. Hu, N. Gao, A.A. Al-Ghamdi, X. Fang, Adv. Funct. Mater. 24 (2014) 3725.
[40] H. Zhang, Y. Zhu, J. Phys. Chem. C 114 (2010) 5822.
[41] B. Pan, Y. Xie, S. Zhang, L. Lv, W. Zhang, ACS Appl. Mater. Interfaces 4 (2012) 3938.
[42] Y. Hu, X. Gao, L. Yu, Y. Wang, J. Ning, S. Xu, X.W. Lou (Eds.), Angew. Chem. Int. 52 (2013) 5636.
[43] L. Ge, F. Zuo, J. Liu, Q. Ma, C. Wang, D. Sun, L. Bartels, P. Feng, J. Phys. Chem. C 116 (2012) 13708.

Please cite this article in press as: Q. Fan, et al., Superior nanoporous graphitic carbon nitride photocatalyst coupled with CdS quantum dots for photodegradation of RhB, Catal. Today (2015), http://dx.doi.org/10.1016/j.cattod.2015.08.006

[44] S.-W. Cao, Y.-P. Yuan, J. Fang, M.M. Shahjamali, F.Y.C. Boey, J. Barber, S.C. Joachim Loo, C. Xue, Int. J. Hydrogen Energy 38 (2013) 1258.
[45] J. Fu, B. Chang, Y. Tian, F. Xi, X. Dong, J. Mater. Chem. A 1 (2013) 3083.
[46] Z. Fang, H. Rong, Z. Ya, P. Qi, J. Mater. Sci. 50 (2015) 3057.
[47] R.C. Pawar, V. Khare, C.S. Lee, Dalton Trans. 43 (2014) 12514.
[48] J. Zhang, Y. Wang, J. Jin, J. Zhang, Z. Lin, F. Huang, J. Yu, ACS Appl. Mater. Interfaces 5 (2013) 10317.
[49] D. Zheng, G. zhang, X. Wang, Appl. Catal. B: Environ. 179 (2015) 479.
[50] E. Kroke, M. Schwarz, E. Horath-Bordon, P. Kroll, B. Noll, A.D. Norman, New J. Chem. 26 (2002) 508.
[51] B.-H. Min, M.B. Ansari, Y.-H. Mo, S.-E. Park, Catal. Today 204 (2013) 156.
[52] J. Hong, X. Xia, Y. Wang, R. Xu, J. Mater. Chem. 22 (2012) 15006.
[53] Y. Cui, Chin. J. Catal. 36 (2015) 372.

Please cite this article in press as: Q. Fan, et al., Superior nanoporous graphitic carbon nitride photocatalyst coupled with CdS quantum dots for photodegradation of RhB, Catal. Today (2015), http://dx.doi.org/10.1016/j.cattod.2015.08.006